

Observation of $B^0 \rightarrow a_1^\pm(1260)\pi^\mp$

K. Abe,⁹ K. Abe,⁴⁷ I. Adachi,⁹ H. Aihara,⁴⁹ K. Aoki,²³ K. Arinstein,² Y. Asano,⁵⁴
T. Aso,⁵³ V. Aulchenko,² T. Aushev,¹³ T. Aziz,⁴⁵ S. Bahinipati,⁵ A. M. Bakich,⁴⁴
V. Balagura,¹³ Y. Ban,³⁶ S. Banerjee,⁴⁵ E. Barberio,²² M. Barbero,⁸ A. Bay,¹⁹ I. Bedny,²
U. Bitenc,¹⁴ I. Bizjak,¹⁴ S. Blyth,²⁵ A. Bondar,² A. Bozek,²⁹ M. Bračko,^{9, 21, 14}
J. Brodzicka,²⁹ T. E. Browder,⁸ M.-C. Chang,⁴⁸ P. Chang,²⁸ Y. Chao,²⁸ A. Chen,²⁵
K.-F. Chen,²⁸ W. T. Chen,²⁵ B. G. Cheon,⁴ C.-C. Chiang,²⁸ R. Chistov,¹³ S.-K. Choi,⁷
Y. Choi,⁴³ Y. K. Choi,⁴³ A. Chuvikov,³⁷ S. Cole,⁴⁴ J. Dalseno,²² M. Danilov,¹³ M. Dash,⁵⁶
L. Y. Dong,¹¹ R. Dowd,²² J. Dragic,⁹ A. Drutskoy,⁵ S. Eidelman,² Y. Enari,²³ D. Epifanov,²
F. Fang,⁸ S. Fratina,¹⁴ H. Fujii,⁹ N. Gabyshev,² A. Garmash,³⁷ T. Gershon,⁹ A. Go,²⁵
G. Gokhroo,⁴⁵ P. Goldenzweig,⁵ B. Golob,^{20, 14} A. Gorišek,¹⁴ M. Grosse Perdekamp,³⁸
H. Guler,⁸ R. Guo,²⁶ J. Haba,⁹ K. Hara,⁹ T. Hara,³⁴ Y. Hasegawa,⁴² N. C. Hastings,⁴⁹
K. Hasuko,³⁸ K. Hayasaka,²³ H. Hayashii,²⁴ M. Hazumi,⁹ T. Higuchi,⁹ L. Hinz,¹⁹ T. Hojo,³⁴
T. Hokuue,²³ Y. Hoshi,⁴⁷ K. Hoshina,⁵² S. Hou,²⁵ W.-S. Hou,²⁸ Y. B. Hsiung,²⁸
Y. Igarashi,⁹ T. Iijima,²³ K. Ikado,²³ A. Imoto,²⁴ K. Inami,²³ A. Ishikawa,⁹ H. Ishino,⁵⁰
K. Itoh,⁴⁹ R. Itoh,⁹ M. Iwasaki,⁴⁹ Y. Iwasaki,⁹ C. Jacoby,¹⁹ C.-M. Jen,²⁸ R. Kagan,¹³
H. Kakuno,⁴⁹ J. H. Kang,⁵⁷ J. S. Kang,¹⁶ P. Kapusta,²⁹ S. U. Kataoka,²⁴ N. Katayama,⁹
H. Kawai,³ N. Kawamura,¹ T. Kawasaki,³¹ S. Kazi,⁵ N. Kent,⁸ H. R. Khan,⁵⁰
A. Kibayashi,⁵⁰ H. Kichimi,⁹ H. J. Kim,¹⁸ H. O. Kim,⁴³ J. H. Kim,⁴³ S. K. Kim,⁴¹
S. M. Kim,⁴³ T. H. Kim,⁵⁷ K. Kinoshita,⁵ N. Kishimoto,²³ S. Korpar,^{21, 14} Y. Kozakai,²³
P. Krizan,^{20, 14} P. Krokovny,⁹ T. Kubota,²³ R. Kulasiri,⁵ C. C. Kuo,²⁵ H. Kurashiro,⁵⁰
E. Kurihara,³ A. Kusaka,⁴⁹ A. Kuzmin,² Y.-J. Kwon,⁵⁷ J. S. Lange,⁶ G. Leder,¹²
S. E. Lee,⁴¹ Y.-J. Lee,²⁸ T. Lesiak,²⁹ J. Li,⁴⁰ A. Limosani,⁹ S.-W. Lin,²⁸ D. Liventsev,¹³
J. MacNaughton,¹² G. Majumder,⁴⁵ F. Mandl,¹² D. Marlow,³⁷ H. Matsumoto,³¹
T. Matsumoto,⁵¹ A. Matyja,²⁹ Y. Mikami,⁴⁸ W. Mitaroff,¹² K. Miyabayashi,²⁴ H. Miyake,³⁴
H. Miyata,³¹ Y. Miyazaki,²³ R. Mizuk,¹³ D. Mohapatra,⁵⁶ G. R. Moloney,²² T. Mori,⁵⁰
A. Murakami,³⁹ T. Nagamine,⁴⁸ Y. Nagasaka,¹⁰ T. Nakagawa,⁵¹ I. Nakamura,⁹
E. Nakano,³³ M. Nakao,⁹ H. Nakazawa,⁹ Z. Natkaniec,²⁹ K. Neichi,⁴⁷ S. Nishida,⁹
O. Nitoh,⁵² S. Noguchi,²⁴ T. Nozaki,⁹ A. Ogawa,³⁸ S. Ogawa,⁴⁶ T. Ohshima,²³ T. Okabe,²³
S. Okuno,¹⁵ S. L. Olsen,⁸ Y. Onuki,³¹ W. Ostrowicz,²⁹ H. Ozaki,⁹ P. Pakhlov,¹³ H. Palka,²⁹
C. W. Park,⁴³ H. Park,¹⁸ K. S. Park,⁴³ N. Parslow,⁴⁴ L. S. Peak,⁴⁴ M. Pernicka,¹²
R. Pestotnik,¹⁴ M. Peters,⁸ L. E. Piilonen,⁵⁶ A. Poluektov,² F. J. Ronga,⁹ N. Root,²
M. Rozanska,²⁹ H. Sahoo,⁸ M. Saigo,⁴⁸ S. Saitoh,⁹ Y. Sakai,⁹ H. Sakamoto,¹⁷
H. Sakaue,³³ T. R. Sarangi,⁹ M. Satapathy,⁵⁵ N. Sato,²³ N. Satoyama,⁴² T. Schietinger,¹⁹
O. Schneider,¹⁹ P. Schönmeier,⁴⁸ J. Schümann,²⁸ C. Schwanda,¹² A. J. Schwartz,⁵
T. Seki,⁵¹ K. Senyo,²³ R. Seuster,⁸ M. E. Sevier,²² T. Shibata,³¹ H. Shibuya,⁴⁶ J.-G. Shiu,²⁸
B. Shwartz,² V. Sidorov,² J. B. Singh,³⁵ A. Somov,⁵ N. Soni,³⁵ R. Stamen,⁹ S. Stanič,³²
M. Starič,¹⁴ A. Sugiyama,³⁹ K. Sumisawa,⁹ T. Sumiyoshi,⁵¹ S. Suzuki,³⁹ S. Y. Suzuki,⁹
O. Tajima,⁹ N. Takada,⁴² F. Takasaki,⁹ K. Tamai,⁹ N. Tamura,³¹ K. Tanabe,⁴⁹
M. Tanaka,⁹ G. N. Taylor,²² Y. Teramoto,³³ X. C. Tian,³⁶ S. N. Tovey,²² K. Trabelsi,⁸
Y. F. Tse,²² T. Tsuboyama,⁹ T. Tsukamoto,⁹ K. Uchida,⁸ Y. Uchida,⁹ S. Uehara,⁹

T. Uglov,¹³ K. Ueno,²⁸ Y. Unno,⁹ S. Uno,⁹ P. Urquijo,²² Y. Ushiroda,⁹ G. Varner,⁸
 K. E. Varvell,⁴⁴ S. Villa,¹⁹ C. C. Wang,²⁸ C. H. Wang,²⁷ M.-Z. Wang,²⁸ M. Watanabe,³¹
 Y. Watanabe,⁵⁰ L. Widhalm,¹² C.-H. Wu,²⁸ Q. L. Xie,¹¹ B. D. Yabsley,⁵⁶ A. Yamaguchi,⁴⁸
 H. Yamamoto,⁴⁸ S. Yamamoto,⁵¹ Y. Yamashita,³⁰ M. Yamauchi,⁹ Heyoung Yang,⁴¹
 J. Ying,³⁶ S. Yoshino,²³ Y. Yuan,¹¹ Y. Yusa,⁴⁸ H. Yuta,¹ S. L. Zang,¹¹ C. C. Zhang,¹¹
 J. Zhang,⁹ L. M. Zhang,⁴⁰ Z. P. Zhang,⁴⁰ V. Zhilich,² T. Ziegler,³⁷ and D. Zürcher¹⁹

(The Belle Collaboration)

¹*Aomori University, Aomori*

²*Budker Institute of Nuclear Physics, Novosibirsk*

³*Chiba University, Chiba*

⁴*Chonnam National University, Kwangju*

⁵*University of Cincinnati, Cincinnati, Ohio 45221*

⁶*University of Frankfurt, Frankfurt*

⁷*Gyeongsang National University, Chinju*

⁸*University of Hawaii, Honolulu, Hawaii 96822*

⁹*High Energy Accelerator Research Organization (KEK), Tsukuba*

¹⁰*Hiroshima Institute of Technology, Hiroshima*

¹¹*Institute of High Energy Physics,*

Chinese Academy of Sciences, Beijing

¹²*Institute of High Energy Physics, Vienna*

¹³*Institute for Theoretical and Experimental Physics, Moscow*

¹⁴*J. Stefan Institute, Ljubljana*

¹⁵*Kanagawa University, Yokohama*

¹⁶*Korea University, Seoul*

¹⁷*Kyoto University, Kyoto*

¹⁸*Kyungpook National University, Taegu*

¹⁹*Swiss Federal Institute of Technology of Lausanne, EPFL, Lausanne*

²⁰*University of Ljubljana, Ljubljana*

²¹*University of Maribor, Maribor*

²²*University of Melbourne, Victoria*

²³*Nagoya University, Nagoya*

²⁴*Nara Women's University, Nara*

²⁵*National Central University, Chung-li*

²⁶*National Kaohsiung Normal University, Kaohsiung*

²⁷*National United University, Miao Li*

²⁸*Department of Physics, National Taiwan University, Taipei*

²⁹*H. Niewodniczanski Institute of Nuclear Physics, Krakow*

³⁰*Nippon Dental University, Niigata*

³¹*Niigata University, Niigata*

³²*Nova Gorica Polytechnic, Nova Gorica*

³³*Osaka City University, Osaka*

³⁴*Osaka University, Osaka*

³⁵*Panjab University, Chandigarh*

³⁶*Peking University, Beijing*

³⁷*Princeton University, Princeton, New Jersey 08544*

³⁸*RIKEN BNL Research Center, Upton, New York 11973*

- ³⁹*Saga University, Saga*
⁴⁰*University of Science and Technology of China, Hefei*
⁴¹*Seoul National University, Seoul*
⁴²*Shinshu University, Nagano*
⁴³*Sungkyunkwan University, Suwon*
⁴⁴*University of Sydney, Sydney NSW*
⁴⁵*Tata Institute of Fundamental Research, Bombay*
⁴⁶*Toho University, Funabashi*
⁴⁷*Tohoku Gakuin University, Tagajo*
⁴⁸*Tohoku University, Sendai*
⁴⁹*Department of Physics, University of Tokyo, Tokyo*
⁵⁰*Tokyo Institute of Technology, Tokyo*
⁵¹*Tokyo Metropolitan University, Tokyo*
⁵²*Tokyo University of Agriculture and Technology, Tokyo*
⁵³*Toyama National College of Maritime Technology, Toyama*
⁵⁴*University of Tsukuba, Tsukuba*
⁵⁵*Utkal University, Bhubaneswer*
⁵⁶*Virginia Polytechnic Institute and State University, Blacksburg, Virginia 24061*
⁵⁷*Yonsei University, Seoul*

Abstract

We report a new measurement of the branching fraction of neutral B meson decays $B^0 \rightarrow a_1^\pm(1260)\pi^\mp$ with $a_1^\pm(1260) \rightarrow \rho^0\pi^\pm$ and $\rho^0 \rightarrow \pi^+\pi^-$ using 275×10^6 $B\bar{B}$ pairs collected by the Belle detector at the KEKB asymmetric-energy e^+e^- collider. We measure the branching fraction $\mathcal{B}(B^0 \rightarrow a_1^\pm(1260)\pi^\mp) = (48.6 \pm 4.1(stat) \pm 3.9(syst)) \times 10^{-6}$. Using a relativistic Breit-Wigner parameterization, we measure the mass and width of the $a_1(1260)$ to be $m_{a_1} = 1197 \pm 34$ MeV/ c^2 and $\Gamma_{a_1} = 305 \pm 43$ MeV/ c^2 , respectively.

PACS numbers: 13.25.HW, 11.30.Er, 12.15.Hh, 14.40.Nd

The Kobayashi and Maskawa (KM) model explains the source of CP violation in terms of a single complex phase in the quark mixing matrix [1]. Measurements of the CP violating asymmetry parameter $\sin 2\phi_1$ by the Belle [2] and BaBar [3] collaborations have established CP violation in the neutral B meson system. Measurements of other CP violating asymmetry parameters provide important tests of the KM model. Decay modes where the $b \rightarrow u\bar{u}d$ contribution is dominant, such as $B^0 \rightarrow \pi^+\pi^-$, $B^0 \rightarrow \rho\pi$, $B^0 \rightarrow \rho\rho$ and $B^0 \rightarrow a_1\pi$ can be used to measure the Cabibbo-Kobayashi-Maskawa angle ϕ_2 (also denoted α) [4]. Unlike $B^0 \rightarrow \pi^+\pi^-$ decay, $B^0 \rightarrow a_1^+\pi^-$ decay is not a CP eigenstate, and four flavor-charge configurations ($B^0(\bar{B}^0) \rightarrow a_1^\pm\pi^\mp$) must be considered to measure the angle ϕ_2 .

The CLEO collaboration has quoted an upper limit of 49×10^{-5} at the 90% C.L. for the branching fraction of $B^0 \rightarrow a_1^\pm(1260)\pi^\mp$ [5], while the DELPHI collaboration has given an upper limit of 28×10^{-5} for the branching fraction of $B^0 \rightarrow 4\pi$ at the 90% C.L. [6]. Recently the BaBar collaboration has reported a measured branching fraction of $\mathcal{B}(B^0 \rightarrow a_1^\pm(1260)\pi^\mp) = (40.2 \pm 3.9(stat) \pm 3.9(syst)) \times 10^{-6}$ [7]. In some previous studies discrepancies have been found in the $a_1(1260)$ properties. Among these studies, the analyses involving hadronic events [8] and τ decays [9] are important. Therefore, it is important to measure the branching fraction of this decay mode. A new precise measurement of the $a_1(1260)$ properties is also useful.

We present in this paper a measurement of the branching fraction of $B^0 \rightarrow a_1^\pm(1260)\pi^\mp$ with $a_1^\pm(1260) \rightarrow \rho^0\pi^\pm$ and $\rho^0 \rightarrow \pi^+\pi^-$ [10]. In this analysis, we assume that the main contributions come from the $B^0 \rightarrow a_1^\pm(1260)\pi^\mp$ and $B^0 \rightarrow a_2^\pm(1320)\pi^\mp$ decays, and neglect any interferences between decay modes consisting of four charged pions in the final state. We also assume that $a_1(1260)$ decays to $\rho\pi$ only.

The analysis is based on a 253 fb^{-1} data sample containing 275 million $B\bar{B}$ pairs. The data were collected with the Belle detector [11] at the KEKB asymmetric-energy e^+e^- (3.5 on 8 GeV) collider [12] operating at the $\Upsilon(4S)$ resonance ($\sqrt{s} = 10.58 \text{ GeV}$) with a peak luminosity that exceeds $1.5 \times 10^{34} \text{ cm}^{-2}\text{s}^{-1}$. The Belle detector is a large-solid-angle magnetic spectrometer that consists of a silicon vertex detector (SVD), a 50-layer central drift chamber (CDC), an array of aerogel threshold Čerenkov counters (ACC), a barrel-like arrangement of time-of-flight scintillation counters (TOF) and an electromagnetic calorimeter comprised of CsI(Tl) crystals located inside a super-conducting solenoid coil that provides a 1.5 T magnetic field. An iron flux-return located outside the coil is instrumented to detect K_L^0 mesons and to identify muons. Two inner detector configurations were used. A 2.0 cm radius beam pipe and a 3-layer silicon vertex detector were used for the first sample of 152 million $B\bar{B}$ pairs, while the remaining 123 million $B\bar{B}$ pairs were recorded using a 1.5 cm radius beam pipe, a 4-layer silicon detector and a small-cell inner drift chamber [13].

For the present analysis several Monte-Carlo (MC) samples (signal and backgrounds) are generated with EvtGen [14]. The Belle detector response is simulated with a GEANT3-based program [15].

We reconstruct the $B^0 \rightarrow a_1^\pm(1260)\pi^\mp$ candidate using four charged tracks originating from the beam interaction region and each having a momentum transverse to the beam, p_t , greater than $100 \text{ MeV}/c$. To identify K and π mesons, we form a $K(\pi)$ likelihood $L_K(L_\pi)$ by combining information from the CDC (dE/dx), the TOF and the ACC. Discrimination between pions and kaons is achieved through the likelihood ratio $R(K/\pi) = L_K/(L_\pi + L_K)$. Charged tracks with $R(K/\pi) < 0.4$ are regarded as pions. Positively identified electrons and muons are rejected.

In the event selection we reconstruct each ρ^0 candidate by combining a π^+ and a π^-

such that the invariant mass of the pion pair ($m_{\pi^+\pi^-}$) satisfies $0.55 \text{ GeV}/c^2 < m_{\pi^+\pi^-} < 1.15 \text{ GeV}/c^2$. We reconstruct the $a_1^\pm(1260)$ candidates by combining another charged pion with the reconstructed ρ^0 . The $a_1^\pm(1260)$ candidates are then selected on the invariant mass: $0.80 \text{ GeV}/c^2 < m_{a_1} < 1.775 \text{ GeV}/c^2$.

Candidate B mesons are identified using three kinematic variables: the beam-energy-constrained mass, $M_{bc} = \sqrt{E_{\text{beam}}^2 - p_B^2}$, the energy difference, $\Delta E = E_B - E_{\text{beam}}$, and the helicity angle of the $a_1(1260)$ meson. Here, E_B and p_B are the reconstructed energy and momentum of the B candidate in the center of mass (c.m.) frame, and E_{beam} is the beam energy in the c.m. frame. The angle between the ρ^0 momentum vector and the direction opposite to the B^0 in the $a_1^\pm(1260)$ rest frame is defined as the helicity angle (θ_{hel}). To extract the signal yield we select events in the region $5.21 \text{ GeV}/c^2 < M_{bc} < 5.29 \text{ GeV}/c^2$, $-0.10 \text{ GeV} < \Delta E < 0.12 \text{ GeV}$ and $-1.0 < \cos \theta_{\text{hel}} < 1.0$ (loose signal region). The momentum of the bachelor pion (the pion that comes directly from the decay of $B^0 \rightarrow a_1^\pm(1260)\pi^\mp$) in the B^0 rest frame is required to satisfy $2.2 \text{ GeV}/c < p_{\text{bach}} < 2.7 \text{ GeV}/c$. We find 39% of the reconstructed events have more than one B candidate after all selection requirements. We select the best B meson candidate that has the minimum χ^2 value in the vertex fit to the four charged pion tracks.

We find 14% of signal events in the MC simulation are incorrectly reconstructed by including at least one charged track from the other B meson. The remaining 86% of signal events are reconstructed from the correct set of final state pions. However there remains the possibility of incorrectly assigning the final state pions to the intermediate mesons in the decay. We find 17% of events have multiple allowable pion combinations. If multiple combinations exist which satisfy the invariant mass constraint on the ρ^0 and $a_1^\pm(1260)$ mesons, we choose the combination such that the daughter pions of the ρ^0 have the larger transverse momenta. With this selection, the probability of selecting the wrong ρ^0 and $a_1^\pm(1260)$ combination is found to be 27% in the signal MC simulation.

The dominant background in the $B^0 \rightarrow a_1^\pm(1260)\pi^\mp$ candidates comes from the continuum $e^+e^- \rightarrow q\bar{q}$ ($q = u, d, s, c$) processes, since the final states contain only charged pions. To suppress the continuum background we apply a Likelihood Ratio (LR) cut. The correlated event shape variables are put into a Fisher discriminant [16] to form a single variable, which is combined with the cosine of the angle between the B meson flight direction and the beam axis, to form a LR. We determine the LR cut value of $LR > 0.80$ by optimizing the figure-of-merit as a function of the LR . From MC studies we find that this cut ($LR > 0.80$) reduces the continuum and $b \rightarrow c$ generic decay backgrounds by 97.4% and 76.6%, respectively.

We estimate the background contribution from rare $b \rightarrow u$ decays using large (2500 fb $^{-1}$ equivalent) MC samples. Since the $B^0 \rightarrow a_2^\pm(1320)\pi^\mp$ decay also has a four pion final state, a significant background contribution is expected from this decay mode. The $a_1(1260)$ meson has a mass of $1.230 \text{ GeV}/c^2$ and a width of $0.25\text{--}0.60 \text{ GeV}/c^2$, whereas the $a_2(1320)$ has a mass of $1.318 \text{ GeV}/c^2$ and a width of $0.107 \text{ GeV}/c^2$ [17]. The upper limit for the branching fraction of $B^0 \rightarrow a_2^\pm(1320)\pi^\mp$ is given as 3.0×10^{-4} (90% C.L.) [17]. From MC studies, we find that the $a_2(1320)$ has a large overlap with the $a_1(1260)$ in the $m_{3\pi}$ distribution, where $m_{3\pi}$ is the invariant mass of three pions. However, since the spins of $a_1(1260)$ and $a_2(1320)$ are different, the helicity angle distributions for the $a_1(1260)$ and $a_2(1320)$ mesons differ. A three dimensional (3D) (M_{bc} - ΔE - $\cos \theta_{\text{hel}}$) fit to the data is used to discriminate the signal from the $a_2(1320)$ background. We note that this method is nearly independent of assumptions about the masses and widths of the $a_1(1260)$ and $a_2(1320)$ mesons.

The signal yields are extracted from a 3D (M_{bc} - ΔE - $\cos \theta_{\text{hel}}$) unbinned maximum likeli-

hood (ML) fit to the data. We fit to the candidates in the loose signal region. We define the likelihood function as:

$$\begin{aligned} \mathcal{L} = \prod_i & \left[f_{a_1\pi} (P_{a_1\pi}(M_{bc i}).P_{a_1\pi}(\Delta E_i).P_{a_1\pi}(\cos \theta_{hel i})) \right. \\ & + f_{a_2\pi} (P_{a_2\pi}(M_{bc i}).P_{a_2\pi}(\Delta E_i).P_{a_2\pi}(\cos \theta_{hel i})) \\ & + f_{b \rightarrow u} (P_{b \rightarrow u}(M_{bc i}).P_{b \rightarrow u}(\Delta E_i).P_{b \rightarrow u}(\cos \theta_{hel i})) \\ & \left. + f_{(q\bar{q}+b \rightarrow c)} (P_{(q\bar{q}+b \rightarrow c)}(M_{bc i}).P_{(q\bar{q}+b \rightarrow c)}(\Delta E_i).P_{(q\bar{q}+b \rightarrow c)}(\cos \theta_{hel i})) \right], \quad (1) \end{aligned}$$

where i runs over all events in the sample. The coefficients $f_{a_1\pi}$, $f_{a_2\pi}$, $f_{b \rightarrow u}$ and $f_{(q\bar{q}+b \rightarrow c)}$ denote the fractions of events from $B^0 \rightarrow a_1^\pm(1260)\pi^\mp$ signal, $B^0 \rightarrow a_2^\pm(1320)\pi^\mp$ background, charmless rare $b \rightarrow u$ decay background and continuum and generic decay ($q\bar{q} + b \rightarrow c$) background, respectively.

The $P(M_{bc i})$, $P(\Delta E_i)$ and $P(\cos \theta_{hel i})$ are the Probability Density Functions (PDFs) in M_{bc} , ΔE and $\cos \theta_{hel}$ for the signal and background contributions, respectively. The PDF for the $B^0 \rightarrow a_1^\pm(1260)\pi^\mp$ signal is taken from a MC simulation, with the calibration correction obtained from the $B^0 \rightarrow D^-\pi^+$, $D^- \rightarrow K^+\pi^-\pi^-$ control sample. The M_{bc} and ΔE signal PDFs are described with a double Gaussian function and the $\cos \theta_{hel}$ signal PDF with a third order polynomial function. The PDFs for continuum and $b \rightarrow c$ decays are taken from the sideband data, where the M_{bc} sideband region is defined as $5.21 \text{ GeV}/c^2 < M_{bc} < 5.26 \text{ GeV}/c^2$, and the ΔE sideband region is defined as $0.10 \text{ GeV} < \Delta E < 0.35 \text{ GeV}$. The shapes of the M_{bc} , ΔE and $\cos \theta_{hel}$ distributions for the sideband data are assumed to be the same for continuum and generic $b \rightarrow c$ backgrounds. This assumption is justified using a MC simulation. The M_{bc} , ΔE and $\cos \theta_{hel}$ PDFs for continuum and generic $b \rightarrow c$ backgrounds are an ARGUS function, a second order polynomial and a third order polynomial, respectively. The PDF for $B^0 \rightarrow a_2^\pm(1320)\pi^\mp$ background is also taken from a MC simulation. The M_{bc} and ΔE shapes are modelled as a single Gaussian and the $\cos \theta_{hel}$ distribution is described by a 4th order polynomial function. The $b \rightarrow u$ background PDF is taken from MC samples.

In the fit we float the $f_{a_1\pi}$, $f_{a_2\pi}$ and $f_{b \rightarrow u}$ coefficients and constrain $f_{(q\bar{q}+b \rightarrow c)}$ according to $f_{(q\bar{q}+b \rightarrow c)} = 1 - (f_{a_1\pi} + f_{a_2\pi} + f_{b \rightarrow u})$. Figure 1 shows the projections of the M_{bc} , ΔE and $\cos \theta_{hel}$ distribution. The M_{bc} plot shows the projection with $-0.04 \text{ GeV} < \Delta E < 0.04 \text{ GeV}$, the ΔE plot shows the projection with $5.27 \text{ GeV}/c^2 < M_{bc} < 5.29 \text{ GeV}/c^2$ and the $\cos \theta_{hel}$ plot shows the projection with $5.27 \text{ GeV}/c^2 < M_{bc} < 5.29 \text{ GeV}/c^2$ and $-0.04 \text{ GeV} < \Delta E < 0.04 \text{ GeV}$ (tight signal region).

A total of 13541 events survive after all the selection requirements and are included in the fit. From the fit we find 394 ± 33 $B^0 \rightarrow a_1^\pm(1260)\pi^\mp$ signal events, 34 ± 38 $B^0 \rightarrow a_2^\pm(1320)\pi^\mp$ background events and 26 ± 30 rare decay background events. The remaining events in the fit are from continuum and generic $b \rightarrow c$ background.

We calculate the branching fraction using the following equation:

$$\mathcal{B}(B^0 \rightarrow a_1^\pm(1260)\pi^\mp) = \frac{N_{a_1^\pm\pi^\mp}}{N_{B\bar{B}} \cdot \varepsilon \cdot Br^{sub} \cdot \varepsilon_{PID}}, \quad (2)$$

where $N_{a_1^\pm\pi^\mp}$ is the number of $B^0 \rightarrow a_1^\pm(1260)\pi^\mp$ events obtained from the M_{bc} - ΔE - $\cos \theta_{hel}$ simultaneous fit, $N_{B\bar{B}}$ is the number of $B\bar{B}$ pairs, Br^{sub} is the branching fraction of the $a_1^\pm(1260)$ decay, ε is the reconstruction efficiency estimated from MC, and ε_{PID} is the correction for the difference in particle identification (PID) efficiency for pions between data

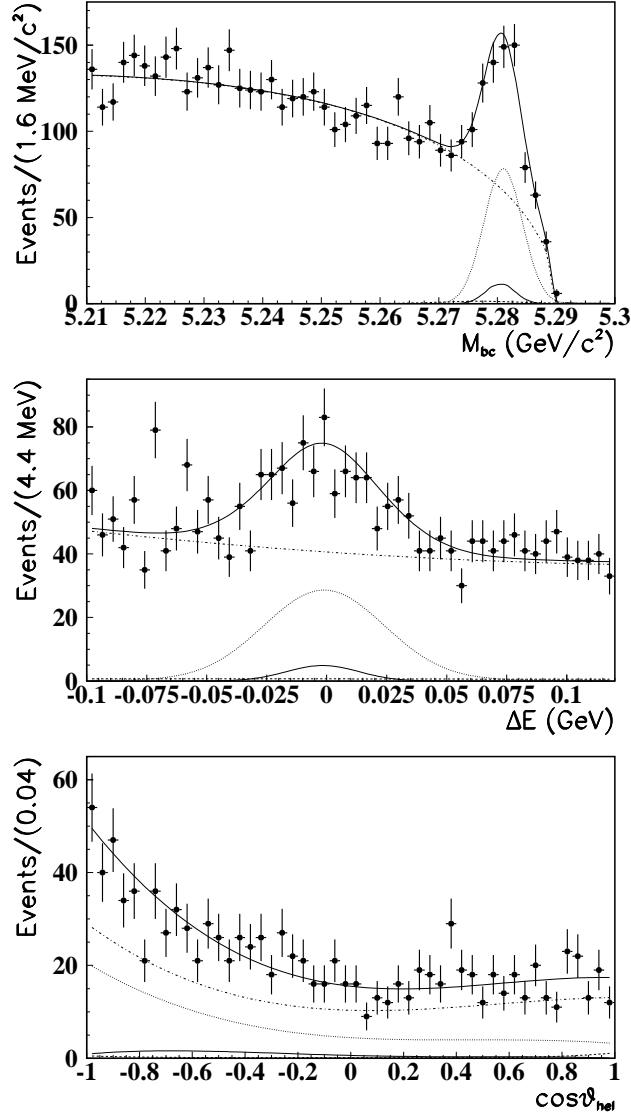


FIG. 1: M_{bc} , ΔE and $\cos\theta_{hel}$ projections for the 3D unbinned ML fit for the selected sample. The top, middle and bottom figures show the M_{bc} , ΔE and $\cos\theta_{hel}$ distributions, respectively. In each plot, the top solid line, the dotted dash line, the dotted line, the bottom solid line and the bottom dash line represent the total fit function, the continuum background, the signal yield, the $B^0 \rightarrow a_2^\pm(1320)\pi^\mp$ background and the rare decay background, respectively.

and a MC simulation. The estimated values for ε and ε_{PID} are 0.061 and 0.962, respectively. The branching fraction of $a_1^\pm(1260) \rightarrow \rho^0 \pi^\pm$ decay is assumed to be 0.5.

Inserting all these values in Eq. (2) we measure the branching fraction $\mathcal{B}(B^0 \rightarrow a_1^\pm(1260)\pi^\mp) = (48.6 \pm 4.1(stat)) \times 10^{-6}$.

To measure the $a_1(1260)$ properties (mass and width) and the contribution from the non-resonant components, we select 1193 $B^0 \rightarrow a_1^\pm(1260)\pi^\mp$ candidates with the tight signal region to enhance signal events. We fit the $a_1(1260)$ mass within the mass window $0.8 \text{ GeV}/c^2 < m_{3\pi} < 1.775 \text{ GeV}/c^2$. For the $m_{3\pi}$ fit, we use the following likelihood function:

$$\mathcal{L} = \prod_i \left[f_{a_1\pi} P_{a_1\pi}(m_{3\pi}^i) + f_{a_2\pi} P_{a_2\pi}(m_{3\pi}^i) + f_{b \rightarrow u} P_{b \rightarrow u}(m_{3\pi}^i) + f_{(q\bar{q}+b \rightarrow c)} P_{(q\bar{q}+b \rightarrow c)}(m_{3\pi}^i) \right], \quad (3)$$

where i runs over all events. The coefficients $f_{a_1\pi}$, $f_{a_2\pi}$, $f_{b \rightarrow u}$, and $f_{(q\bar{q}+b \rightarrow c)}$ represent fractions of events from signal, $B^0 \rightarrow a_2^\pm(1320)\pi^\mp$ background, $b \rightarrow u$ background and $(q\bar{q} + b \rightarrow c)$ background, respectively. The $P(m_{3\pi})$ are the PDFs for the corresponding signal and background contributions. In the present analysis we impose several kinematical cuts in the event selection, which produce a non-uniform efficiency in $m_{3\pi}$. We obtain an efficiency correction curve from a MC simulation, which is applied to the relativistic Breit-Wigner (RBW) function for the $a_1(1260)$ and $a_2(1320)$ PDFs. The sideband events and MC are used to determine the background shapes for $(q\bar{q} + b \rightarrow c)$ and $b \rightarrow u$, respectively. The PDFs for the $(q\bar{q} + b \rightarrow c)$ and $b \rightarrow u$ backgrounds are 5th and 6th order polynomial functions, respectively. In the fit we fix the fractions of $B^0 \rightarrow a_1^\pm(1260)\pi^\mp$, $B^0 \rightarrow a_2^\pm(1320)\pi^\mp$ and $b \rightarrow u$ to those obtained from the 3D $M_{bc}-\Delta E-\cos\theta_{\text{hel}}$ fit [18]. We allow the mean and width of the $a_1^\pm(1260)$ RBW function to float in the fit, while those of $a_2^\pm(1320)$ are fixed to the world averages [17]. Figure 2 shows the $m_{3\pi}$ and ρ^0 mass distributions for the events that survive after the tight signal region cut. From the fit we determine the mass and width of the $a_1(1260)$ as $1197 \pm 34(\text{stat})$ MeV/ c^2 and $305 \pm 43(\text{stat})$ MeV/ c^2 , respectively.

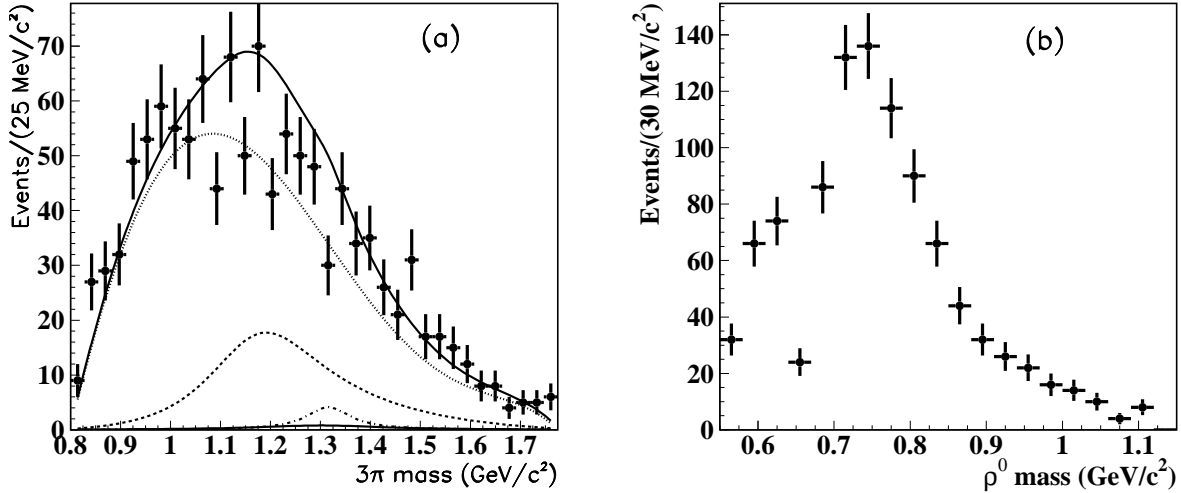


FIG. 2: (a) $m_{3\pi}$ and (b) ρ^0 mass distributions for the events in the tight signal region. In plot (a) the top solid line shows the total fit, the dotted line shows the contribution from $q\bar{q} + b \rightarrow c$, the dashed line shows the contribution from $B^0 \rightarrow a_1^\pm(1260)\pi^\mp$, the dotted-dashed line shows the contribution from $B^0 \rightarrow a_2^\pm(1320)\pi^\mp$ and the bottom solid line represents the contribution from the $b \rightarrow u$ background.

In order to measure the non-resonant components, we extend the likelihood function of Eq. (3) by adding non-resonant contributions from $B^0 \rightarrow \rho^0\pi^+\pi^-$ and $B^0 \rightarrow \pi^+\pi^-\pi^+\pi^-$.

The extended likelihood function includes the additional coefficients $f_{\rho\pi\pi}$ and $f_{4\pi}$ which represent the fractions of the non-resonant $B^0 \rightarrow \rho^0\pi^+\pi^-$ and $B^0 \rightarrow \pi^+\pi^-\pi^+\pi^-$ decays, respectively. The PDFs for $B^0 \rightarrow \rho^0\pi^+\pi^-$ and $B^0 \rightarrow \pi^+\pi^-\pi^+\pi^-$ decays are taken from MC. We perform the $m_{3\pi}$ fit in the $0.80 \text{ GeV}/c^2 < m_{3\pi} < 1.775 \text{ GeV}/c^2$ range to extract the non-resonant components. In the fit we fix the $b \rightarrow u$ and $(q\bar{q} + b \rightarrow c)$ fractions to those obtained from the $M_{bc}\text{-}\Delta E\text{-}\cos\theta_{\text{hel}}$ fit. We also fix the values for the mean and width of the $a_1(1260)$ to $1230 \text{ MeV}/c^2$ and $300 \text{ MeV}/c^2$, respectively, which lies in the world average limits [17]. We apply the constraint: $1 - f_{b \rightarrow u} - f_{(q\bar{q} + b \rightarrow c)} = f_{a_1\pi} + f_{a_2\pi} + f_{\rho\pi\pi} + f_{4\pi}$. Thus there are four free parameters in the fit: $f_{a_1\pi}$, $f_{a_2\pi}$, $f_{\rho\pi\pi}$ and $f_{4\pi}$. We combine the $f_{\rho\pi\pi}$ and $f_{4\pi}$ fractions and estimate the total non-resonant component from $B^0 \rightarrow \rho^0\pi^+\pi^-$ and $B^0 \rightarrow \pi^+\pi^-\pi^+\pi^-$. We obtain a non-resonant component fraction of $5.3 \pm 5.4\%$, which is consistent with 0. Accordingly, we include the non-resonant contribution as a systematic error in the branching fraction measurement.

The measured signal yield from the 3D fit contains several systematic uncertainties. The systematic error in the signal yield is estimated by varying each parameter of the fit by $\pm 1\sigma$ from the nominal values. The shifts in the signal yields are then added in quadrature. The corresponding uncertainties are listed in Table I. We assign the uncertainty in the track reconstruction efficiency to be $\pm 4.8\%$. We measure the uncertainty in the efficiency of the PID selection of the charged pions to be $\pm 1.4\%$. A systematic error of -5.3% is assigned to a potential contribution from the non-resonant $B \rightarrow 4\pi$ and $B \rightarrow \rho\pi\pi$ decays. For the selection of the LR cut, a systematic error of $+2.7\%$ and -2.3% is measured. We estimate the uncertainty in the number of $B\bar{B}$ pairs to be $\pm 1.1\%$. For the efficiency calculation with MC we assign a systematic error of $\pm 0.5\%$. The reconstruction efficiency (ε) is estimated with MC simulation generated with $m_{a_1} = 1230 \text{ MeV}/c^2$ and $\Gamma_{a_1} = 400 \text{ MeV}/c^2$. We vary the m_{a_1} and Γ_{a_1} to our measured values and estimate the efficiency variation, and find that the difference is -0.5% . We thus add it as a systematic error. We also vary the ΔE range for the 3D fit to check possible variation of background contribution. The ΔE is varied from $-0.10 \text{ GeV} < \Delta E < 0.10 \text{ GeV}$ to $-0.30 \text{ GeV} < \Delta E < 0.30 \text{ GeV}$. We find $+4.3\%$ and -1.6% signal yield variation and assign it to the systematic error. Finally, we add a $+1.8\%$ systematic error for the fit bias. The total systematic error is $+7.8\%$ and -8.1% . The branching fraction is measured to be $\mathcal{B}(B^0 \rightarrow a_1^\pm(1260)\pi^\mp) = (48.6 \pm 4.1(\text{stat}) \pm 3.9(\text{syst})) \times 10^{-6}$.

As a validity check of the procedure in the present analysis we measure the branching fraction of the $B^0 \rightarrow D^-\pi^+, D^- \rightarrow K^+\pi^-\pi^-$ decay. For this check we perform a $M_{bc}\text{-}\Delta E$ unbinned maximum likelihood fit to obtain the signal yield. The branching fraction is measured to be $(2.46 \pm 0.05) \times 10^{-3}$, which is consistent with the world average value of $(2.76 \pm 0.25) \times 10^{-3}$ [17].

In conclusion, we have performed a new measurement of the branching fraction for the decay, $B^0 \rightarrow a_1^\pm(1260)\pi^\mp$, with $a_1^\pm(1260) \rightarrow \rho^0\pi^\pm$ and $\rho^0 \rightarrow \pi^+\pi^-$. Based on a 253 fb^{-1} data sample, the measured branching fraction is $\mathcal{B}(B^0 \rightarrow a_1^\pm(1260)\pi^\mp) = (48.6 \pm 4.1(\text{stat}) \pm 3.9(\text{syst})) \times 10^{-6}$, which is consistent with the BaBar measurement [7]. Fitting with an efficiency corrected relativistic Breit-Wigner, we measure the parameters of the $a_1(1260)$ to be $m_{a_1} = 1197 \pm 34 \text{ MeV}/c^2$ and $\Gamma_{a_1} = 305 \pm 43 \text{ MeV}/c^2$. These values are consistent with the BaBar measurement [7] and the world average values [17].

We thank the KEKB group for the excellent operation of the accelerator, the KEK cryogenics group for the efficient operation of the solenoid, and the KEK computer group

TABLE I: Systematic errors for the $M_{bc}\text{-}\Delta E\text{-}\cos\theta_{\text{hel}}$ fit.

Source of the systematic error	Relative error (%)	
	$+\sigma$	$-\sigma$
Track reconstruction efficiency	4.8	-4.8
PID efficiency	1.4	-1.4
Fraction of the non-resonant components	0.0	-5.3
Continuum suppression cut	2.7	-2.3
Signal shape	1.3	-0.9
$B^0 \rightarrow a_2^\pm(1320)\pi^\mp$ background shape	0.4	-0.3
Continuum background shape	1.7	-1.5
Rare decay background shape	0.4	-0.4
Number of $B\bar{B}$	1.1	-1.1
MC statistics	0.5	-0.5
m_{a_1} parameters in MC	0.0	-0.5
ΔE cut selection	4.3	-1.6
Fit bias	1.8	-0.0
Total	7.8	-8.1

and the National Institute of Informatics for valuable computing and Super-SINET network support. We acknowledge support from the Ministry of Education, Culture, Sports, Science, and Technology of Japan and the Japan Society for the Promotion of Science; the Australian Research Council and the Australian Department of Education, Science and Training; the National Science Foundation of China under contract No. 10175071; the Department of Science and Technology of India; the BK21 program of the Ministry of Education of Korea and the CHEP SRC program of the Korea Science and Engineering Foundation; the Polish State Committee for Scientific Research under contract No. 2P03B 01324; the Ministry of Science and Technology of the Russian Federation; the Ministry of Higher Education, Science and Technology of the Republic of Slovenia; the Swiss National Science Foundation; the National Science Council and the Ministry of Education of Taiwan; and the U.S. Department of Energy.

-
- [1] M. Kobayashi and T. Maskawa, Prog. Theo. Phys. **49**, 652 (1973).
 - [2] Belle Collaboration, K. Abe *et al.*, Phys. Rev. Lett. **89**, 201802 (2002).
 - [3] BaBar Collaboration, B. Aubert *et al.*, Phys. Rev. D **66**, 071102 (2002).
 - [4] R. Aleksan *et al.*, Nucl. Phys. B **361**, 141 (1991).
 - [5] CLEO Collaboration, D. Bortolotto *et al.*, Phys. Rev. Lett. **62**, 2436 (1989).
 - [6] DELPHI Collaboration, P. Abreu *et al.*, Phys. Rev. Lett. **357**, 255 (1995).
 - [7] BaBar Collaboration, B. Aubert *et al.*, hep-ex/0507029 (2005).
 - [8] J. Perneger *et al.*, Nucl. Phys. B **134**, 439 (1978); C. Daum *et al.*, Phys. Lett. B **89**, 281 (1980); D.V. Amelin *et al.*, Phys. Lett. B **356**, 595 (1995).

- [9] D. M. Asner *et al.*, Phys. Rev. D **61**, 012002-1 (1999); P. Abreu *et al.*, Phys. Lett. B **426**, 411 (1998).
- [10] Throughout this paper, the inclusion of $\bar{B}^0 \rightarrow a_1^\pm(1260)\pi^\mp$ decays is implied.
- [11] Belle Collaboration, A. Abashian *et al.*, Nucl. Instr. and Meth. A **479**, 117 (2002).
- [12] S. Kurokawa and E. Kikutani, Nucl. Instrum. Meth. Phys. Res., Sect. A **499**, 1 (2003), and references therein.
- [13] Y. Ushiroda (Belle SVD2 Group), Nucl. Instr. and Meth. A **511**, 6 (2003).
- [14] D. J. Lange, Nucl. Instr. and Meth. A **462**, 152 (2001).
- [15] GEANT - detector description and simulation tool (1993), CERN Program Library Long Writeup W5013.
- [16] Belle Collaboration, K. Abe *et al.*, Phys. Rev. Lett. **87**, 101801 (2001); Belle Collaboration, K. Abe *et al.*, Phys. Lett. **B 511**, 151 (2001).
- [17] Particle Data Group, S. Eidelman *et al.*, Phys. Lett. B **592**, 1 (2004).
- [18] From 3D(M_{bc} - ΔE - $\cos\theta_{hel}$) fit the fractions for the signal and backgrounds are measured. Here we use those fractions with an efficiency correction for the tight signal region cut of m_{a_1} selection ranges.